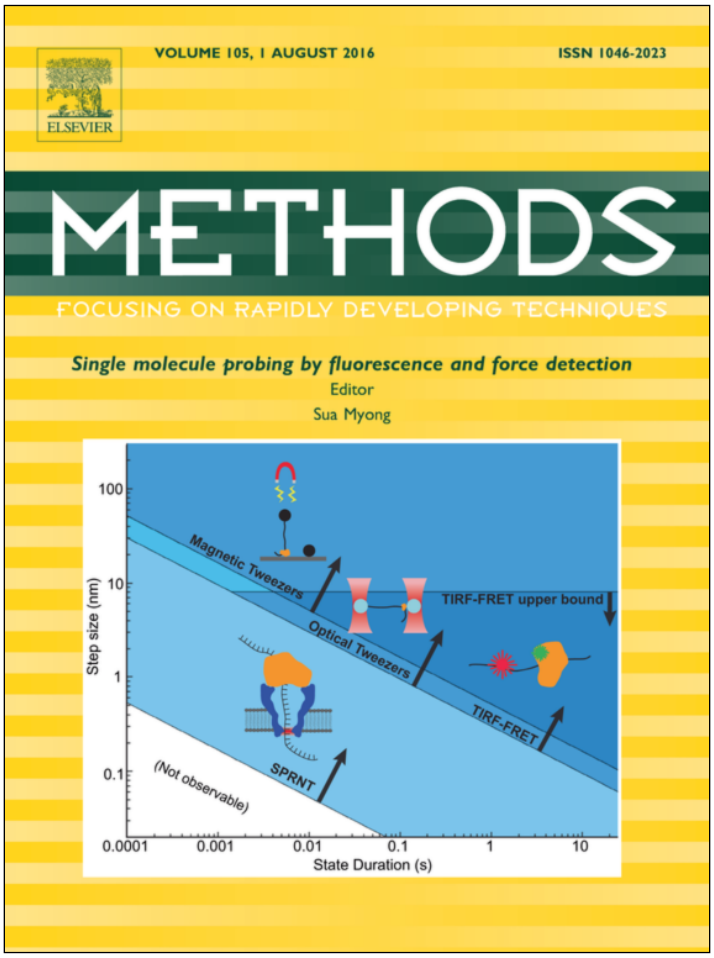

Methods 105 (2016) 90–98

Contents lists available at ScienceDirect

Methods

journal homepage: www.elsevier.com/locate/ymeth

High-throughput, high-force probing of DNA-protein interactions with magnetic tweezers

Bojk A. Berghuis, Mariana Köber, Theo van Laar, Nynke H. Dekker *

Department of Bionanoscience, Kavli Institute of Nanoscience, Faculty of Applied Sciences, Delft University of Technology, Lorentzweg 1, 2628 CJ Delft, The Netherlands

ARTICLE INFO

Article history:
Received 21 December 2015
Received in revised form 23 March 2016
Accepted 29 March 2016
Available online 30 March 2016

Keywords:
Magnetic tweezers
High-throughput
DNA construct design
Tus-Ter
SV40 large T antigen helicase

ABSTRACT

Recent advances in high-throughput single-molecule magnetic tweezers have paved the way for obtaining information on individual molecules as well as ensemble-averaged behavior in a single assay. Here we describe how to design robust high-throughput magnetic tweezers assays that specifically require application of high forces (>20 pN) for prolonged periods of time (>1000 s). We elaborate on the strengths and limitations of the typical construct types that can be used and provide a step-by-step guide towards a high tether yield assay based on two examples. Firstly, we discuss a DNA hairpin assay where force-induced strand separation triggers a tight interaction between DNA-binding protein Tus and its binding site *Ter*, where forces up to 90 pN for hundreds of seconds were required to dissociate Tus from *Ter*. Secondly, we show how the LTag helicase of Simian virus 40 unwinds dsDNA, where a load of 36 pN optimizes the assay readout. The approaches detailed here provide guidelines for the high-throughput, quantitative study of a wide range of DNA-protein interactions.

1. Introduction

In recent decades, single-molecule techniques have become a valuable addition to existing bulk assays to study biological processes. The direct access to reaction kinetics has proven to provide crucial insights into the stochastic behavior and transient dynamics of individual molecules [1–6]. An additional challenge is to efficiently build up statistics in order to correctly place the occurrence of individual events in perspective of the total distribution of events. A single-molecule technique well equipped for this challenge is magnetic tweezers (MT), especially since recent developments in hardware and data acquisition software have paved the way to perform hundreds of single-molecule experiments simultaneously [7,8].

In any magnetic tweezers assay, single molecules are used to tether micrometer-sized magnetic beads to the surface of a fluid chamber. The beads are visualized through a microscope objective, and the resulting image is recorded with a camera (Fig. 1a). The properties of the individual molecules are inferred through the movement of the beads: continuously in motion due to Brownian motion of the surrounding water molecules, but limited in their movement as a result of the anchoring via the molecule of interest. An increased upward pulling force induced by lowering a pair of magnets towards the fluid chamber stretches the tethers and limits bead movement even further. It is this force-extension relationship that is molecule-specific and can be used to e.g. infer the rate at which a helicase unwinds a double-stranded (ds) DNA helix [9,10].

Choosing the best possible manner through which to read out enzyme activity or the binding of the protein of interest is arguably the single most fundamental and creative part of a single-molecule MT experiment. Most commonly, a DNA tether is used as a means to detect enzyme activity or protein binding in MT experiments. RNA tethers have also been used with great success [8,11–16], but as these form a smaller subset of experiments, for simplicity we focus exclusively on DNA in this article. Given the ease with which DNA can be manipulated using tools of molecular biology, the possibilities for tether design are rich. This has been exemplified by the many creative designs used over the past years [9,10,17–19]. While summing up all designs used to date is beyond the scope of this paper, we identify roughly three classes of DNA constructs: the linear – forked or nicked – dsDNA construct, the rotationally constrained dsDNA construct that allows the introduction of supercoils [20], and the DNA hairpin (Fig. 1b and c).

A linear dsDNA construct is the archetypal manner to tether a bead to a surface as a means to infer the properties of this construct (or the proteins/enzymes interacting with it) through tracking the bead movement through conventional light microscopy (Fig. 2a). The behavior of dsDNA and single-stranded (ss) DNA under applied tension is well studied [9] and can be modeled using

* Corresponding author.
E-mail address: n.h.dekker@tudelft.nl (N.H. Dekker).

http://dx.doi.org/10.1016/j.ymeth.2016.03.025
1046-2023/

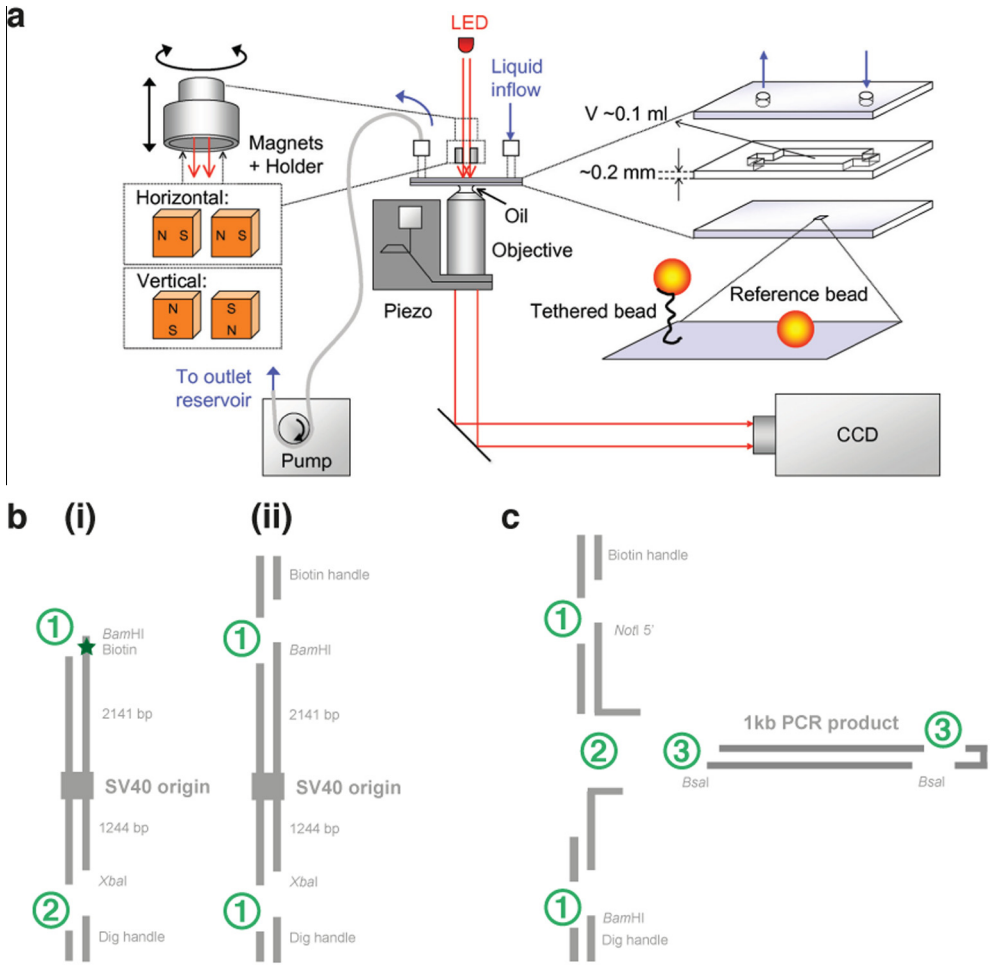

Fig. 1. The magnetic tweezers setup and construct design & assembly. (a) The magnetic tweezers setup: an inverted microscope stage that is used to project the image of surface-tethered beads onto a CCD/CMOS camera chip [51]. (b) Typical design of a torsionally unconstrained (i) and a torsionally constrained (ii) dsDNA construct, different sequential or parallel ligation steps shown (green numbered circles) (c) Design and assembly strategy of the *Ter* DNA hairpin.

the worm-like chain (WLC) model or extensions thereof [21,22]. In detecting enzyme activity or protein binding using a dsDNA construct, the difference in force-extension characteristics between dsDNA and ssDNA is essential (Fig. 2d), as the conversion of the ds helical structure into ssDNA (or protein-covered ssDNA) under force can then be observed as a change in the end-to-end extension of the construct/tether (~0.17 nm/bp at 25 pN). For a nicked or forked construct, the application of force is on one strand and has a destabilizing effect on the double helix, culminating in the overstretching transition to ssDNA at forces around 65 pN [23,24,21]. At lower forces (up to ~35 pN), pulling force is known to assist enzymes in plowing through the double helix, leading to less and shorter stochastic polymerase pausing, for instance [8].

While a forked dsDNA assay suffices in cases where processive enzyme activity or extensive DNA-binding is measured, the readout of e.g. a single protein-binding event or a short burst of activity might be somewhat limited. Here the use of a rotationally constrained dsDNA construct might be more apt (Fig. 2b). At low forces (<1 pN), a reduction of the linking number through the application of negative turns leads to the formation of plectonemic supercoils, and thereby to a decrease in tether extension (Fig. 2e) [25,26]. At higher forces, it results in a reduction of twist and concomitant denaturation [27,28] with initially little change in extension (Fig. 2e) until an increase is observed upon significant underwinding (Fig. 4d). Such a rotationally constrained dsDNA construct can be used e.g. to probe for removal of supercoils by topoisomerases [29–32] or to probe for protein- or enzyme-induced opening up of the double helix, as such increased unwinding leads to a compensatory change in dsDNA extension at low force [3,18]. In the latter case, monitoring changes in the state of DNA supercoiling provides a more sensitive measure of enzymatic activity than simple ds to ss conversion, as also shown by experiments that probe progression of RNA polymerases by monitoring the positive torsional strain they upstream of their location as they move along the DNA [33].

A third class of DNA constructs is the DNA hairpin (Fig. 2c). The use of DNA hairpins has several important advantages compared to dsDNA constructs. First of all, as a DNA hairpin implies exertion of force on both strands of the double helix equally, this becomes a very direct way to measure unwinding activity of the myriad of enzymes equipped to do so. Applying a force lowers the energy barrier the enzyme has to overcome in the most direct way possible, namely by pulling apart the double helix [34]. Secondly, DNA hairpins have a higher resolution in the readout compared to linear dsDNA constructs, as each disruption of a Watson-Crick base pair leads to a jump of two single-stranded inter-base distances (~0.6 nm/bp as opposed to ~0.12 nm/bp at 12 pN for a forked DNA construct) [14,33]. Thirdly, DNA hairpins allow for a direct control over the rehybridization process as the work required to unzip a DNA hairpin is equivalent to the work performed by an

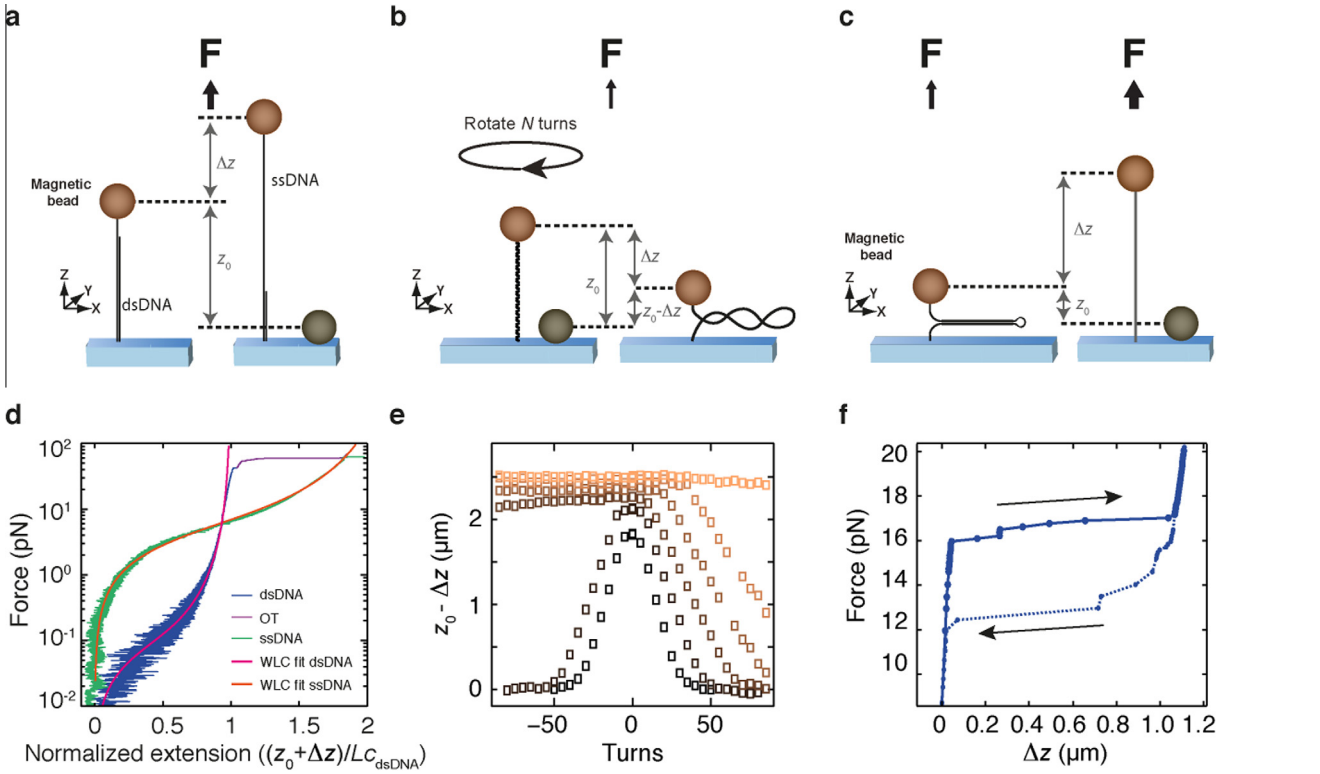

Fig. 2. The magnetic tweezers assays and examples of the achievable readouts. (a) A linear dsDNA construct where only one of the DNA strands is attached to the bead renders it rotationally unconstrained and implies the pulling force is applied on one of the ssDNA strands only (*Lc* = 7.0 kbp). We calibrate the extension change would result from ds to ssDNA conversion through enzymatic activity by measuring the force-extension relationships for dsDNA (blue data) and ssDNA (green data) in separate experiments, as shown in (d). At the overstretching transition (OT, magenta), the force is sufficiently high to allow sudden peeling of the dsDNA helix, such that the tethered strand becomes single-stranded. The difference in electrochemical properties of ds and ssDNA imply that at forces above ~8 pN ds-to-ss conversion yields tether lengthening, while at forces lower than ~8 pN tether shortening would be observed. (b) The application of turns to a torsionally constrained dsDNA (*Lc* = 7.9 kbp). At low forces, plectonemic supercoils (*Wr*) can be introduced by applying turns to a torsionally constrained dsDNA as illustrated schematically. The response of dsDNA to applied rotation at different forces is indicated (e, from dark to light, F = 0.25, 0.5, 1.1, 2, 3.5, and 6.5 pN). (c) A DNA hairpin (*Lc*(haipin stem) = 1.1 kbp) is closed at low forces (<13 pN), so the hairpin extension <Δz> is zero. Increasing the force (>16 pN) will open the hairpin: for every broken base pair, two ssDNA base lengths are added to the tether length. This force extension relationship is also characterized in a force-extension experiment (f).

enzyme performing the unzipping (Fig. 2f). The work needed to melt a linear dsDNA construct lies significantly higher. However, the use of DNA hairpins also comes with certain drawbacks that must be taken into consideration. For example, the unwinding activity of a helicase on a hairpin under low force may not be readily detectable, as the newly exposed ssDNA will form a random coil. Furthermore, the use of hairpins offers no possibility for torsional control (unless there is a third anchoring point [35]) and lastly, there is always tension on an initiation site at or downstream of the fork.

As the DNA construct leaves the drawing board, an often-recurring problem arising in making the DNA construct is low yield of the final product. As there are usually several intermediate products (e.g. biotin- or digoxygenin-labelled handles, hairpin loops, mismatch regions, primers, etc.) that need to be ligated together in one or several steps, the yield is highly dependent on the order through which this happens as well as the choice of the restriction sites/enzymes.

Over recent years, we have refined and improved the method of DNA construct production and assembly, and have come up with a robust method to produce a wide variety of construct designs based on a few fundamental steps. We will elaborate on two different dsDNA constructs as well as a DNA hairpin. Furthermore, as construct yield is the initial of many steps towards tether yield in the experiment, we discuss the subsequent experimental setup and present several strategic choices to be made leading to a successful high-throughput single-molecule experiment, exemplified through a number of typical enzymatic and protein-nucleic acid interaction assays. We first touch upon the assay-specific calibrations necessary to perform the experiments and then elaborate on two protein-DNA interaction assays: an assay where the specific binding and locking of Tus onto a 23 bp *Ter* site is investigated with a DNA hairpin [36], followed by tracking of the enzymatic unwinding activity of the LTag helicase as it unwinds dsDNA.

2. Methods

2.1. Preparation of DNA hairpins

The 1.1 kb Ter hairpins were generated by PCR using plasmids pTER and pTER_Rev as a template, containing the TerB site in either the nonpermissive or permissive orientation, respectively, and flanked by phage λ sequences, were obtained from Invitrogen (Invitrogen/Life Technologies, Carlsbad, CA). The hairpins were constructed in a multistep process, where the specific order of assembly described here contributes significantly to the final product yield (Fig. 1c). First, a 1-kb fragment containing the TerB site was amplified from the pTER plasmid using primers 1 and 2 (Table 1). This fragment was digested with the nonpalindromic restriction enzyme *Bsa*I (New England BioLabs Inc., Ipswich, MA) and ligated at one end to a 42-bp oligonucleotide forming a U-turn (oligonucleotide 3). The hairpin handles were created by PCR amplification of a 1.2-kb pBluescript SK$^+$ (Stratagene–Agilent

Table 1
Oligonucleotides used for the DNA hairpin construct.

Oligo-nucleotide	Sequence
1	5′CTGCGGTCTCGTTGCTTACCGTCACCAGAAATTACCGTCAC3′
2	5′CCATCTTGGTCTCCTAGGTTTTTAGCAGCGAAGCGTTTGATAAG3′
3	5′CCTAAGCTCGCCGAGGCGAGCGAAAGCTCGCCTCGGCGAGCT3′
4	5′GACCGAGATAGGGTTGAGTG3′
5	5′CAGGGTCGGAACAGGAGAGC3′
6	5′GGCAAGAGCAACTCGGTCGCCGCATACACTATTCTCAGAATGACTTGGTT3′
7	5′GGCCAACCAAGTCATTCTGAGAATAGTGTATGCGGCGACCGAGTTGCTCTTGCCATGCTCTTTACAACCGGTTGACTGCTTCAGGGGTCGATCCCGCTTTGTAC3′
8	5′GATCTCGTTCATCCATAGTTGCCTGACTCCCCGTCGTGTAGATAACTACGATACGGGAGGGCTTACCATCTGGC3′
9	5′GCAAGTACAAAGCGGGATCGACCCCTGAAGCAGTCAACCGGTTGTAAAGAGCATCGATCGTTGTCAGAAGTAAGTTGGCCGCAGTGTTATCACTCATGGTTATG CCAGATGGTAAGCCCTCCCGTATCGTAGTTATCTACACGACGGGGAGTCAGGCAACTATGGATGAACGA3′
10	5′CCATCTTGGTCTCCGACATTATAGCACAGTCGTGGTGAC3′
11	5′CTGCGGTCTCGAGGCGGTTAATATTATGGCGCGTTG3′
12	5′P-GCCTACTTTAGTTACAACATACTTATT3′
13	5′P-TGTCAAACCTCATGTTGTAACTAAAGT3′

Technologies, Santa Clara, CA) fragment using primers 4 and 5 in the presence of either biotin-16-dUTP or digoxigenin-11-dUTP (Roche Diagnostics, Basel, Switzerland). Prior to ligation to spacer oligonucleotides, handles were digested with either *Bam*HI or *Not*I. The upper spacer of the hairpin was generated by annealing 5′-phosphorylated oligonucleotides 6 and 7 and ligating this double-stranded DNA fragment to the *Not*I-digested biotin-labelled handle. The lower spacer was made by annealing 5′-phosphorylated primers 8 and 9 and ligating them to the *Bam*HI-digested digoxigenin-labelled handle. Finally, the overhangs of these handle-spacer constructs were allowed to anneal to form a short (50-bp) stem with a 5′-GCAA overhang that was ligated to the complementary *Bsa*I site of the 1-kb TerB fragment. Oligonucleotides were obtained from Biolegio B.V., Nijmegen, the Netherlands and from Ella Biotech GmbH, Martinsried, Germany.

2.2. Preparation of a DNA hairpin containing a mismatch region

To create a 1 kb fragment containing a 5-base mismatch between bases 3–7 in the Ter site, two fragments of 500 bp were generated by PCR using pTER as template and primer combinations 1 and 10, and 2 and 11 (Table 1), respectively. These fragments were digested with *Bsa*I and ligated to each end of the annealed primer pair 12 and 13 containing the wobble.

2.3. Preparation of 3.4 kb dsDNA construct containing the SV40 origin of replication

To monitor enzyme activity, we engineered a torsionally unconstrained 3.4 kb dsDNA construct containing the SV40 origin of replication close to the center of the construct (Fig. 1b, (i)). For calibration purposes, where we mechanically unwind the DNA, we created a torsionally constrained construct (Fig. 1b, (ii)). The design of these constructs is based on the plasmid pRL-SV40 (Promega Corporation, Madison, WI), with handles containing biotin on one end and digoxigenin on the other end. Using restriction sites for *Bam*HI and *Xba*I in the plasmid, a fragment was created with 2141 bp on one side of the SV40 origin and 1244 bp on the other side of the origin. For the torsionally constrained constructs, 600 bp handles containing either biotin or digoxigenin are ligated on the ends. These handles are amplified by PCR from pBluescriptSKII$^+$ using forward primer 5′-GACCGAGATAGGGTTGAGTG and reverse primer 5′-CAGGGTCGGAACAGGAGAGC in the presence of biotin-16-dUTP or digoxigenin-11-dUTP (Roche Diagnostics, Basel, Switzerland) in a ratio of 1:5 with dTTP. Therefore, the expected number of labelled nucleotides is approximately 60 per 600-bp handle. For the torsionally unconstrained construct, pRL-SV40 (Promega Corporation, Madison, WI) was digested with *Bam*HI and the 5′-overhang was filled with Klenow (New England BioLabs Inc., Ipswich, MA) in the presence of biotin-labelled dATP (Invitrogen/Life Technologies, Carlsbad, CA). Subsequently, the DNA was digested with *Xba*I and ligated to a digoxigenin-labelled handle that was digested with *Xba*I as described above.

2.4. Functionalization of flow cell surfaces

Glass microscope cover slips (#1, 24 × 60 mm, Menzel GmbH, Germany) serve as the flow cell surface for DNA anchoring as well as the top for sealing off the flow cell. Inlet/outlet holes were drilled in the top cover slip. Then all cover slips were placed into a Teflon holder and sonicated in acetone for 30 min, followed by another sonication step in 2-propanol for another 30 min, after which they were allowed to air dry. Then the bottom glass surfaces were coated with nitrocellulose. For this, nitrocellulose membrane paper (Invitrogen, USA) was dissolved (1% m/V) in ethanol as a stock by mixing the components in a tube shaker at 35 °C. Prior to use, the nitrocellulose solution was diluted to 0.2% m/V. At this stage polystyrene (3 μm diameter) reference beads can be added to the nitrocellulose solution, the concentration of beads depends on the MT field of view size (typically a ∼1000× dilution is used). Another option would be to add the polystyrene reference beads dissolved in buffer to the flow cell at a later stage. The melting allows for more thorough surface attachment with the risk of having clusters of molten beads on your surface, the addition at a later stage allows for better control, with the risk of losing more beads when flushing. Irrespective of the choice made, 5 min sonication of the polystyrene beads prior to addition is recommended. Functionalization of the flow cell surface is performed by adding 3 μl of the nitrocellulose solution and spreading it out evenly using the lateral side of the pipette tip. If this solution contains reference beads, the cover glasses should be heated to 150 °C for 3 min on hot plate.

2.5. Flow cell assembly and preparation

A double layer of parafilm spacer was placed onto the functionalized surfaces, and the flow cell was closed by a second coverslip on top containing inlet and outlet holes. The cover slip parafilm sandwich was sealed by melting the parts together at 90 °C for ∼30 s. Prior to the addition of DNA-linked magnetic beads, the bottom surface was functionalized by incubation with 1 mg ml^{-1} anti-digoxigenin (Roche) in PBS for 30 min to provide for DNA attachment. The surface was passivated by incubating blocking aid

(an undisclosed mix of proteins from Sigma) for 10 min followed by a 10 min incubation of high salt buffer (e.g. 700 mM KCl).

2.6. Bead tethering and post-incubation cleanup

DNA constructs (final concentration ~ 50 pg/μl) were mixed and incubated for 2 min with 20 μl streptavidin-coated paramagnetic beads (M270 Dynabeads) at room temperature in Tris buffer (50 mM Tris–HCl pH 7.9, 50 mM KCl, 0.1 mM EDTA, 0.01% Triton X-100). Triton X-100 is used to avoid bead clustering. The supernatant was replaced by 50 μl Tris buffer followed by a 15 min incubation of the bead-DNA solution in the flow cell containing an anti-digoxigenin-coated nitrocellulose surface. Non-tethered beads were removed by flushing with 1 ml Tris buffer, applying a high (30–40 pN) force while rotating the magnets (10 turns and back and forth repeatedly at 10 Hz), and followed by flushing with more buffer (at low force (0.1 pN) to keep the removed beads from settling back onto the tethers) until all non-tethered beads had been flushed out.

2.7. Specifications of the magnetic tweezers

The magnetic tweezers implementation used in this study has been previously described [7,8,37]. Briefly, light transmitted through the sample was collected by an oil-immersion objective (Olympus UPLSAPO60XO 60×, numerical aperture (NA) = 1.35, Olympus, USA) and projected onto a 12-megapixel CMOS camera (Falcon FA-80-12M1H, Teledyne Dalsa, Canada) with a sampling frequency of 58 Hz at full field of view, or higher when cropped. A 2-inch 200-mm tube lens between objective and camera resulted in an effective magnification of 67×. As a result of the aforementioned camera and magnification specifications, the field of view (fov) size is approximately 300 × 400 μm, allowing for the possibility of tracking hundreds of beads simultaneously. The applied magnetic field was generated by a pair of vertically aligned permanent neodymium-iron-boron magnets (SuperMagnete, Switzerland) separated by a distance of 1.0 or 0.5 mm and suspended on a motorized stage (M-126.PD2, Physik Instrumente, Germany) above the flow cell. Additionally, the magnet pair could be rotated about the illumination axis by an applied DC servo step motor (C-150.PD, Physik Instrumente, Germany).

2.8. Pre-experiment tether calibrations

2.8.1. Hairpin calibration and testing

Prior to measuring the dwell times of *Ter*-bound Tus on the DNA hairpins, we characterized the two DNA hairpins described above in force-extension experiments. The purpose of the calibration experiments is to check the constructs for their length, the opening force of the bare hairpin and verify the location of the *Ter* site upon the addition of Tus. To obtain the force extension curves we start at low force (~8 pN) and lower the magnet position in a linear fashion until a full opening of the DNA hairpin is observed, and back (Fig. 2c). The linear magnet movement will lead to an exponential force ramp, which for the purpose of this experiment yields a rapid and straightforward qualitative test to check whether the hairpins produce the expected unfolding and folding pattern (Fig. 2f).

2.8.2. Canonical pre-measurement test of dsDNA tethers

For each experiment, we select for DNA tethers that have the expected length by measuring the difference in tether extension between high (>10 pN) and low (<100 fN) forces. At zero force the bead bounces on the flow cell surface, so the lowest measured extension (after filtering appropriately) will define zero extension. At forces above ~10 pN the DNA is fully stretched such that the average extension at this force will yield the tether contour length [8,38].

2.8.3. Data acquisition

Image processing of the collected bead diffraction patterns was used to track the real-time position of both surface-attached reference beads and superparamagnetic beads coupled to DNA tethers in three dimensions. We implemented custom written software in C++, CUDA and LabView (2011, National Instruments Corporation, USA) that is suited for high-throughput tracking in magnetic tweezers [7]. Tracking of the *x*, *y* coordinates is performed using center-of-mass computation followed by a further refinement using the quadrant interpolation algorithm. Localization of the bead's *z*-coordinate is achieved by creating a radial profile using the refined *x*, *y* coordinates and comparing this profile to a prerecorded look-up table of radial profiles. After subtraction of the reference bead position to correct for instrumental drift, the *x*, *y* and *z* positions of the DNA-tethered beads were determined with a spatial accuracy of <3 nm. The upward stretching forces on the DNA tethers by the superparamagnetic beads were calibrated from analysis of the extent of their Brownian motion, whereby spectral corrections were employed to correct for camera blur and aliasing [39,40].

3. Measurement types

We now combine the DNA constructs described above with several measurement approaches, of which all exploit the multiplexing capacity of MT to gain statistics on biologically relevant processes that either have a low yield, or take a long time to acquire. All measurements described here are measurements taken at high forces (>20 pN) for prolonged periods of time (up to ~2000 s). These types of measurements require the combination of M270 beads and vertically aligned magnets with a gap size of 0.3–1 mm [40]. These measurements also strongly benefit from the high anti-digoxigenin concentration used here (1 mg/ml) and tether handles containing multiple digoxigenin- and biotin-dUTP moieties.

3.1. Tus measurements on hpDNA – measuring a single dwell time many times

Recently, we investigated the tight interaction between the DNA binding protein Tus and its cognate DNA-binding sequence *Ter* – the system known to be involved in the termination of DNA replication in *Escherichia coli* [36]. It had previously been argued that the tight interaction was dependent on specific interactions between Tus and the replisome [41]. By using a multiplexed MT DNA hairpin assay (Fig. 2c) to mimic fork progression in the absence of replisome proteins, it was shown that protein–protein interactions were not necessary for tight Tus–*Ter* interactions [36]. Gathering the necessary dwell-time statistics would have been very time-consuming without the ability to multiplex, as strand separation frequently remained blocked at the Tus–*Ter* site for hundreds of seconds.

3.2. Hairpin dwell time measurements

For the purpose of clarity, we here discuss the measurements performed on the hairpin construct that contains the *Ter* site in the blocking (nonpermissive) orientation only. Constant-force dwell time experiments were obtained by lowering the magnets in a linear fashion (10 mm/s) to the desired distance. The dwell time is the time measured between arrival of the magnets at their final position and the further opening of the hairpin from the

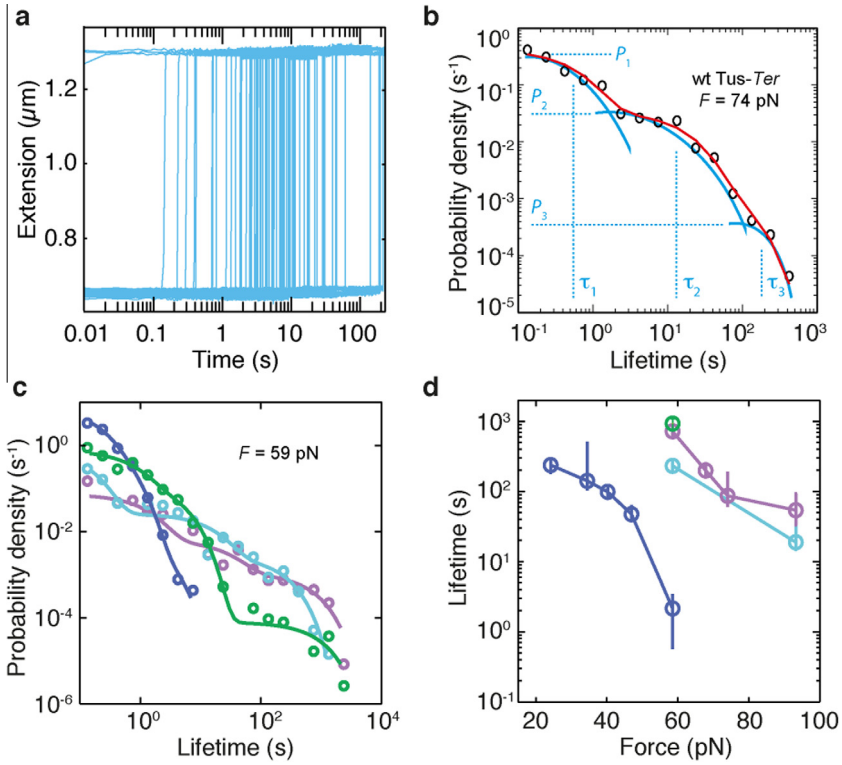

Fig. 3. Experimental readout as well as the resulting dwell time and lifetime distributions of Tus-Ter DNA hairpin experiments. (a) Tus-Ter rupture events on the DNA hairpin construct are marked by a sudden, single jump in the extension, when the hairpin opens from the Ter site (extension = ~0.6 μm) to the fully single-stranded form (ext. = 1.3 μm). Data taken at 74 pN with wt Tus-Ter. (b) The resulting dwell time distribution of the dataset represented in (a), which contains multiple single exponential distributions (global fit in red, guide to the eye in cyan). (c) The dwell-time distributions are altered by mutations in (H144A, blue) or near (E49K, green) the lock domain, but less affected by a mutation elsewhere (Q250A, cyan) when compared to wt Tus-Ter (purple, circles are data, solid lines are fits). (d) The lifetime extracted for the longest-lived state (e.g. tau 3 in (b)) shows that Tus-Ter lock lifetimes depend on force and that a mutation in the lock domain of Tus is what mainly causes a deviation from wt-like behavior (same color scheme as (c), the error bars indicate the 1-σ confidence intervals).

locked to the fully opened state. Rupture of the Tus–*Ter* lock results in a sudden opening of the DNA hairpin (Fig. 3a): rupture points were easily identified as a sharp peak in the derivative of the *z*-trace.

The magnetic tweezers multiplexing capability allows for rapid collection of Tus-*Ter* dwell time distributions (Fig. 3a), as a typical experiment starts out with ~80 DNA hairpins. The dwell times showed to be multi-exponentially distributed. The appropriate number of exponentials required to fit a dataset was determined by applying the Bayes-Schwarz information criterion [42]. Typically three single exponentials were needed to fit a dwell time distribution of Tus-*Ter* [36]. This implies that there are three states in which the Tus-*Ter* lock can find itself trapped, each state with its own characteristic lifetime and probability (Fig. 3b). The longest lived state was found to be the signature of full lock formation, and this state was longest-lived for wt Tus-*Ter*. Mutations in the lock domain led to a decrease in the lifetime and/or probability of this state, while mutations in other Tus domains led to wt-like behavior (Fig. 3c and d).

3.3. Enzymatic activity – LTag unwinding dsDNA – Measuring many dwell times in a single burst of activity

Using our assays, we have also studied the unwinding of duplex DNA by large tumor antigen (LTag) [43], the helicase of the Simian Virus 40 (SV40), which serves as a model system to understand eukaryotic DNA replication [44]. Two LTag hexamers assemble head-to-head at the origin of replication, and subsequently unwind dsDNA bidirectionally. While electron microscopy suggested that the double hexamer may function as a stationary unit that draws in the parental DNA [45], single-molecule fluorescence studies found efficient unwinding by two separate hexamers travelling apart [46]. We have probed whether the two LTag hexamers function as a single unit or not by using magnetic tweezers to investigate LTag-based unwinding with nanometer resolution at high forces (~35 pN). At this force, the extension of ssDNA exceeds that of dsDNA. If the two hexamers separate to unwind the DNA, the creation of ssDNA in an unwinding bubble should (providing absence of rehybridization) result in an increase in tether extension (Fig. 4a). If, on the other hand, DNA is being unwound by a stationary double hexamer that draws in parental DNA, an extension decrease is expected (Fig. 4b). Similarly to the experiments probing Tus binding described above, here we also benefit from the use of high-throughput magnetic tweezers, as they allow us to obtain multiple unwinding traces in a single experiment, limited only by the efficiency of helicase assembly on dsDNA in the flow cell.

3.4. Calibrating the extension change invoked by the formation of an unwinding bubble

To quantify the number of basepairs unwound by the LTag helicase, we need to determine the extension change that results from the unwinding of a dsDNA base pair at a given force. To this end, we mechanically unwind an initially relaxed, but torsionally constrained, DNA (Fig. 4c). This reduces its linking number *Lk*, which is the sum of twist (*Tw*) and writhe (*Wr*). Changes in *Lk*

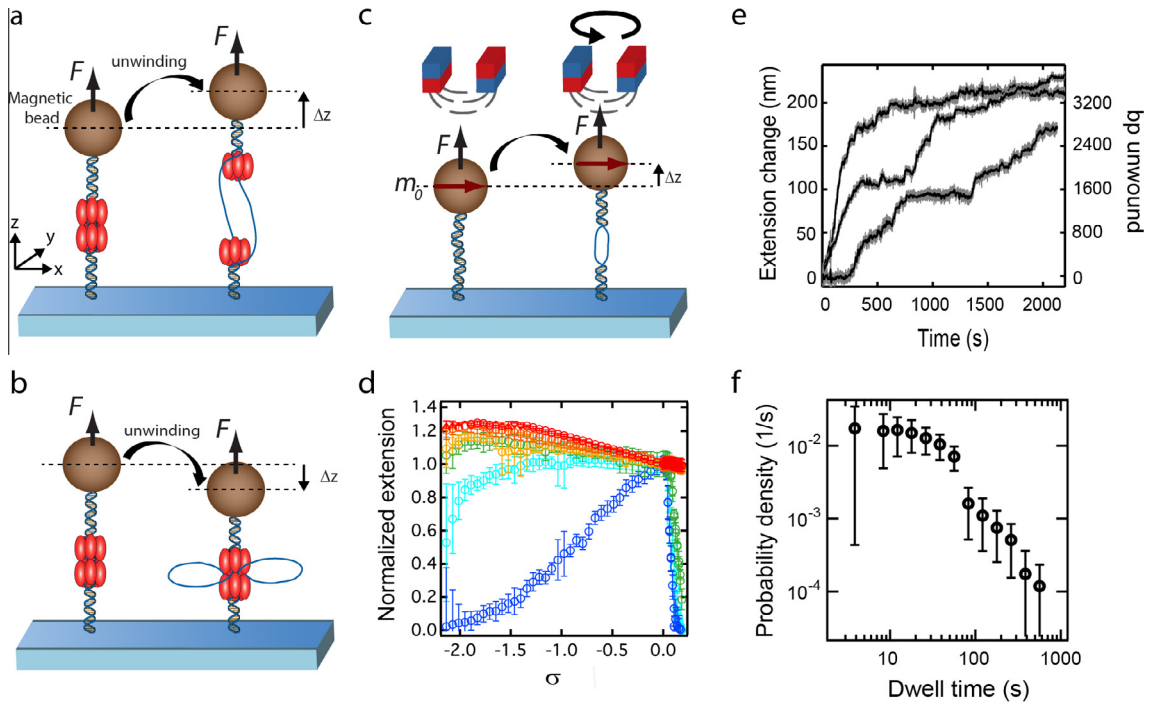

Fig. 4. Experimental readout of LTag unwinding dsDNA containing an origin of replication. (a), (b) Unwinding of dsDNA either by two separate hexamers (a) or by a stationary double hexamer (b). The unwinding of dsDNA by two separating hexamers will create an unwinding bubble. At high forces (>6 pN), this will lead to an extension increase. A stationary double hexamer, on the other hand, will draw in parental dsDNA, and the extension will decrease. (c) To calibrate the extension change that results from the unwinding of a base pair at a given force, we unwind a torsionally constrained DNA molecule mechanically. (d) A reduction of the linking number through the application of negative turns leads to an extension decrease at low force, as a result of the formation of plectonemic supercoils, and to an extension increase at higher forces, due to a reduction of twist and concomitant denaturation (from blue to red, F = 1.2, 2.5, 6, 12, 24, and 36 pN; measurements were performed in 10 mM Tris-HCl, pH 7.4, and 7 mM $MgCl_2$). Fitting the expression $N_u = (\Delta l - a)/b$ to the dataset at 36 pN, we find a = 0.3 nm and b = 0.0625 nm/bp unwound. (e) Typical traces of LTag unwinding different dsDNA molecules. The unwinding yields an extension increase, indicating that under the tested conditions, dsDNA is likely unwound by two separate hexamers as depicted in (a). All three traces shown here were acquired in the presence of 17 nM LTag hexamer and 3 nM RPA. Full-bandwidth traces (acquired at 60 Hz, grey) are shown along with 0.2 Hz low-pass filtered data (black). (f) For a comparison with average unwinding rates reported in literature, we constructed a dwell-time distribution of the dataset shown in (e) with a dwell time window of 200 bp (thus projecting the average unwinding rate over this distance along the template). Error bars are obtained from 1000 bootstrap iterations. From the median of this dwell time distribution, we determine an unwinding rate of 5.2 bp/s at 36 pN.

are conveniently expressed using $\sigma = (Lk - Lk_0)/Lk_0 = (\Delta Tw + Wr)/Lk_0$, where Lk_0 is the linking number of torsionally relaxed DNA [47]. When we reduce σ from 0 to −2 at low forces (<1 pN), this primarily results in the formation of plectonemic supercoils (negative *Wr*) and thereby to a decrease in tether extension (Fig. 4d, e.g. blue data). A similar decrease of σ at higher forces yields a decrease in *Tw* and concomitant denaturation [28,50], resulting in a gradual extension increase (Fig. 4d, e.g. red data). At the highest forces probed (36 pN), the unwinding of duplex DNA leads to a significant increase in DNA extension. Fitting the expression $N_u = (\Delta l - a)/b$ to this dataset (for $-1.7 < \sigma < 0$), where N_u is the number of unwound basepairs, allows us to calculate the degree of unwinding of this 3.4 kb construct from the change in DNA extension Δ*l*, and provides the basis for probing LTag unwinding.

3.5. DNA unwinding by LTag helicase

To monitor DNA unwinding by LTag helicase, we approached the magnets to the flow cell to apply the desired force. 17 nM LTag hexamer was introduced into the flow cell in a buffer containing 10 mM Tris-HCl, pH 7.4, and 7 mM $MgCl_2$, supplemented with 6 mM adenosine triphosphate (ATP), 0.1 mg/mL bovine serum albumin (BSA), 1 mM dithiothreitol (DTT), and 6.8 nM competitor DNA (linearized plasmid pUC19, 2.7 kbp) to impede origin-independent unwinding [48]. After 45 min, 3 nM human replication protein A (RPA) was added in the same buffer to stabilize newly formed ssDNA, supplemented with 6 mM ATP, 0.1 mg/mL BSA, and 1 mM DTT.

Under these conditions, we observed activity-associated increases in the extension for ~1/3 of the DNA tethers present in the flow cell (Fig. 4e), with remaining tethers showing no activity, likely due to absent or inefficient helicase loading. LTag processivity is low in the absence of RPA, which is most likely due to a poor stabilization of ssDNA by LTag alone. In the presence of RPA, however, we mostly observe complete LTag-mediated DNA unwinding (Fig. 4e). For the traces showing activity, we constructed a dwell-time distribution (Fig. 4f). From the median of this dwell-time distribution, we determine an unwinding rate for LTag helicase of 5.2 bp/s at 36 pN (Fig. 4f), which is slightly higher than previously reported average rates [46,49]. These rates were, however, deduced at lower forces (Yardimci et al. report 3.6 ± 0.4 bp/s for DNA tethers stretched to 85–90% of their contour length, implying a tensile stretching force of ~1–2 pN), and quite possibly the unwinding rate is force-dependent. Thus, this establishes an assay with which we can probe the unwinding of dsDNA by LTag starting from an origin of replication. Notably, in our high force experiments, we never observed a decrease in the extension of the DNA tethers. This suggests that, under the probed high-force conditions, two spatially separated LTag hexamers unwind the dsDNA (compare Fig. 4a and b). This observation does not rule out the possibility that at low force conditions LTag mediated DNA unwinding occurs in a head-to-head dimer configuration. Future experiments will be required to determine whether this unwinding mechanism is similarly applied at lower forces.

3.6. Tips

- o If the yield of the DNA construct is low, it is advisable to reconsider the order in which different fragments are ligated.
- o The use of non-palindromic restriction enzymes (e.g. BsaI) avoids self-ligation of the PCR products or primers, resulting in an increased construct yield.
- o Two easy to change factors contribute significantly to DNA tether strength: the Anti-dig concentration (a higher concentration implies stronger tethering) and the DNA-digoxygenin/biotin handle length (the longer, the more anchoring points).
- o Pre-experiment cleanup: avoid being too careful with the tethers (weakly bound tethers will add to mid-experiment failures).
- o Post-experiment cleanup: after performing the experiment, flush through a low-salt buffer through in high-speed bursts (if needed combined with tapping the tubing connected to the flow cell): this will remove all the tethers and stuck beads, the flow cell is ready for another round of experiments.
- o Keep the occasions where air bubbles enter the flow cell chamber to a minimum: this will increase the lifetime of the flow cell.
- o Add detergent (e.g. Triton X-100, 0.01% v/v) to buffers to avoid (reference) bead clustering. After the post incubation cleanup buffers lacking detergent (proteins might be sensitive to detergent) can be used.
- o Keep in mind the reference bead size (bigger is better).

4. Concluding remarks

Here we have described detailed protocols and methods for performing high force, multiplexed MT measurements. Improvements on the design of DNA constructs allow us to producing the DNA constructs with a high yield, which directly translates into a high DNA tether yield in the MT assay. We have drastically reduced tether loss caused by prolonged exposure to high forces (20–95 pN) by using long (600 bp) dsDNA handles labelled with multiple digoxygenin or biotin labels and by increasing the anti-digoxygenin concentration on the flow cell surface. By performing multiplexed measurements on DNA hairpins containing a single nonpermissive *Ter* site we were able to capture the distribution of dwell times that arises from the rupture of the wt Tus-*Ter* lock and various Tus mutants. Using a dsDNA molecule containing the origin of replication for the LTag helicase, we show that the dsDNA is unwound by two separate hexamers. These experiments demonstrate that the MT instrumentation and protocols described here have reached a level where performing multiplexed, high force single-molecule assays has become routine to such an extent that bridging the gap between the dynamics of a single molecule and the ensemble-averaged behavior is now within the realm of possibility.

Acknowledgments

We thank Kollol Aguan, Marijn Versteegh for preliminary experiments, and we thank David Dulin for advice and efforts in protocol development. Purified LTag protein was kindly supplied by the laboratory of Xiaojiang Chen (University of Southern California). This study was supported by a VICI grant from the Netherlands Organisation for Scientific Research (NWO) and an ERC Grant (DynGenome) from the European Research Council, both to N.H.D.

References

[1] A.M. van Oijen, J.J. Loparo, Single-molecule studies of the replisome, Annu. Rev. Biophys. 39 (2010) 429–448.
[2] A.N. Kapanidis, E. Margeat, S.O. Ho, E. Kortkhonjia, S. Weiss, R.H. Ebright, Initial transcription by RNA polymerase proceeds through a DNA-scrunching mechanism, Science 314 (2006) 1144–1147.
[3] A. Revyakin, C. Liu, R.H. Ebright, T.R. Strick, Abortive initiation and productive initiation by RNA polymerase involve DNA scrunching, Science 314 (2006) 1139–1143.
[4] M.H. Larson, R. Landick, S.M. Block, Single-molecule studies of RNA polymerase: one singular sensation, every little step it takes, Mol. Cell 41 (2011) 249–262.
[5] C. Bustamante, W. Cheng, Y.X. Mejia, Revisiting the central dogma one molecule at a time, Cell 144 (2011) 480–497.
[6] C.E. Aitken, A. Petrov, J.D. Puglisi, Single ribosome dynamics and the mechanism of translation, Annu. Rev. Biophys. 39 (2010) 491–513.
[7] J.P. Cnossen, D. Dulin, N.H. Dekker, An optimized software framework for real-time, high-throughput tracking of spherical beads, Rev. Sci. Instrum. 85 (2014) 103712.
[8] D. Dulin, Elongation-competent pauses govern the fidelity of a viral RNA-dependent RNA polymerase, Cell Rep. (2015).
[9] Carlos Bustamante, Zev Bryant, Steven B. Smith, Ten years of tension: single-molecule DNA mechanics, Nature 421 (6921) (2003) 423–427.
[10] T. Lionnet, DNA mechanics as a tool to probe helicase and translocase activity, Nucleic Acids Res. 34 (2006) 4232–4244.
[11] J. Liphardt, B. Onoa, S.B. Smith, I. Tinoco Jr, C. Bustamante, Reversible unfolding of single RNA molecules by mechanical force, Science 292 (2001) 733–737.
[12] J.A. Abels, F. Moreno-Herrero, T. Van der Heijden, C. Dekker, N.H. Dekker, Single-molecule measurements of the persistence length of double-stranded RNA, Biophys. J . 88 (4) (2005) 2737–2744.
[13] S. Dumont, W. Cheng, V. Serebrov, R.K. Beran, I. Tinoco, A.M. Pyle, C. Bustamante, RNA translocation and unwinding mechanism of HCV NS3 helicase and its coordination by ATP, Nature 439 (7072) (2006) 105–108.
[14] W. Cheng, S.G. Arunajadai, J.R. Moffitt, I. Tinoco, C. Bustamante, Single-base pair unwinding and asynchronous RNA release by the hepatitis C virus NS3 helicase, Science 333 (6050) (2011) 1746–1749.
[15] J.D. Wen, L. Lancaster, C. Hodges, A.C. Zeri, S.H. Yoshimura, H.F. Noller, I. Tinoco, Following translation by single ribosomes one codon at a time, Nature 452 (7187) (2008) 598–603.
[16] Jan Lipfert et al., Double-stranded RNA under force and torque: similarities to and striking differences from double-stranded DNA, Proc. Natl. Acad. Sci. 43 (2014) 15408–15413.
[17] J. Gore, Z. Bryant, M.D. Stone, M. Nöllmann, N.R. Cozzarelli, C. Bustamante, Mechanochemical analysis of DNA gyrase using rotor bead tracking, Nature 439 (7072) (2006) 100–104.
[18] Andrey Revyakin, Richard H. Ebright, Terence R. Strick, Promoter unwinding and promoter clearance by RNA polymerase: detection by single-molecule DNA nanomanipulation, Proc. Natl. Acad. Sci. U.S.A. 101 (14) (2004) 4776–4780.
[19] Zev Bryant, Florian C. Oberstrass, Aakash. Basu, Recent developments in single-molecule DNA mechanics, Curr. Opin. Struct. Biol. 22 (3) (2012) 304–312.
[20] D. Dulin, J. Lipfert, M.C. Moolman, N.H. Dekker, Studying genomic processes at the single-molecule level: introducing the tools and applications, Nat. Rev. Genet. 14 (1) (2013) 9–22.
[21] P. Gross, N. Laurens, L.B. Oddershede, U. Bockelmann, E.J. Peterman, G.J. Wuite, Quantifying how DNA stretches, melts and changes twist under tension, Nat. Phys. 7 (9) (2011) 731–736.
[22] C. Bouchiat, M.D. Wang, J.F. Allemand, T. Strick, S.M. Block, V. Croquette, Estimating the persistence length of a worm-like chain molecule from force-extension measurements, Biophys. J . 76 (1) (1999) 409–413.
[23] Steven B. Smith, Yujia. Cui, Carlos. Bustamante, Overstretching B-DNA: the elastic response of individual double-stranded and single-stranded DNA molecules, Science 271 (5250) (1996) 795–799.
[24] P. Cluzel, A. Lebrun, C. Heller, R. Lavery, J.L. Viovy, D. Chatenay, F. Caron, DNA: an extensible molecule, Science 271 (5250) (1996) 792–794.
[25] J. Lipfert, J.W. Kerssemakers, T. Jager, N.H. Dekker, Magnetic torque tweezers: measuring torsional stiffness in DNA and RecA-DNA filaments, Nat. Methods 7 (2010) 977–980.
[26] H. Meng, J. Bosman, T. van der Heijden, J. van Noort, Coexistence of twisted, plectonemic, and melted DNA in small topological domains, Biophys. J . 106 (5) (2014) 1174–1181.
[27] J.F. Allemand, D. Bensimon, R. Lavery, V. Croquette, Stretched and overwound DNA forms a Pauling-like structure with exposed bases, Proc. Natl. Acad. Sci. 95 (24) (1998) 14152–14157.
[28] M.Y. Sheinin, S. Forth, J.F. Marko, M.D. Wang, Underwound DNA under tension: structure, elasticity, and sequence-dependent behaviors, Phys. Rev. Lett. 107 (10) (2011) 108102.
[29] Terence R. Strick, Vincent. Croquette, David. Bensimon, Single-molecule analysis of DNA uncoiling by a type II topoisomerase, Nature 404 (6780) (2000) 901–904.
[30] N.H. Dekker, V.V. Rybenkov, M. Duguet, N.J. Crisona, N.R. Cozzarelli, D. Bensimon, V. Croquette, The mechanism of type IA topoisomerases, Proc. Natl. Acad. Sci. 99 (19) (2002) 12126–12131.
[31] D.A. Koster, V. Croquette, C. Dekker, S. Shuman, N.H. Dekker, Friction and torque govern the relaxation of DNA supercoils by eukaryotic topoisomerase IB, Nature 434 (7033) (2005) 671–674.
[32] D.A. Koster, K. Palle, E.S. Bot, M.A. Bjornsti, N.H. Dekker, Antitumour drugs impede DNA uncoiling by topoisomerase I, Nature 448 (7150) (2007) 213–217.

[33] Y. Harada, O. Ohara, A. Takatsuki, H. Itoh, N. Shimamoto, K. Kinosita, Direct observation of DNA rotation during transcription by *Escherichia coli* RNA polymerase, Nature 409 (6816) (2001) 113–115.
[34] N. Ribeck, D.L. Kaplan, I. Bruck, O.A. Saleh, DnaB helicase activity is modulated by DNA geometry and force, Biophys. J . 99 (7) (2010) 2170–2179.
[35] J.T. Inman, B.Y. Smith, M.A. Hall, R.A. Forties, J. Jin, J.P. Sethna, M.D. Wang, DNA Y structure: a versatile, multidimensional single molecule assay, Nano Lett. 14 (11) (2014) 6475–6480.
[36] B.A. Berghuis, D. Dulin, Z.Q. Xu, T. van Laar, B. Cross, R. Janissen, N.H. Dekker, Strand separation establishes a sustained lock at the Tus-Ter replication fork barrier, Nat. Chem. Biol. 11 (8) (2015) 579–585.
[37] R. Janissen et al., Invincible DNA tethers: covalent DNA anchoring for enhanced temporal and force stability in magnetic tweezers experiments, Nucleic Acids Res. 42 (2014) e137.
[38] Daniel Klaue, Ralf Seidel, Torsional stiffness of single superparamagnetic microspheres in an external magnetic field, Phys. Rev. Lett. 102 (2) (2009) 028302.
[39] A.J.W. Velthuis, J.W.J. Kerssemakers, J. Lipfert, N.H. Dekker, Quantitative guidelines for force calibration through spectral analysis of magnetic tweezers data, Biophys. J. 99 (2010) 1292–1302.
[40] Z. Yu et al., A force calibration standard for magnetic tweezers, Rev. Sci. Instrum. 85 (2014) 123114.
[41] D. Bastia, S. Zzaman, G. Krings, M. Saxena, X. Peng, M.M. Greenberg, Replication termination mechanism as revealed by Tus-mediated polar arrest of a sliding helicase, Proc. Natl. Acad. Sci. 105 (35) (2008) 12831–12836.
[42] G. Schwarz, Estimating dimension of a model, Ann. Statist. 6 (1978) 461–464.
[43] D. Li, R. Zhao, W. Lilyestrom, D. Gai, R. Zhang, J.A. DeCaprio, E. Fanning, A. Jochimiak, G. Szakonyi, X.S. Chen, Structure of the replicative helicase of the oncoprotein SV40 large tumour antigen, Nature 423 (2003) 512.
[44] Ellen Fanning, Kun Zhao, SV40 DNA replication: from the A gene to a nanomachine, Virology 384 (2) (2009) 352–359.
[45] R. Wessel, J. Schweizer, H. Stahl, Simian Virus 40 T-Antigen DNA helicase is a hexamer which forms a binary complex during bidirectional unwinding from the viral origin of DNA replication, J. Virol. 66 (1992) 804.
[46] H. Yardimci, X. Wang, A.B. Loveland, I. Tappin, D.Z. Rudner, J. Hurwitz, A.M. van Oijen, J.C. Walter, Bypass of a protein barrier by a replicative helicase, Nature 492 (2012) 205.
[47] T.Christian Boles, James H. White, Nicholas R. Cozzarelli, Structure of plectonemically supercoiled DNA, J. Mol. Biol. 213 (4) (1990) 931–951.
[48] G.S. Goetz, F.B. Dean, J. Hurwitz, S.W. Matson, The unwinding of duplex regions in DNA by the simian virus 40 large tumor antigen-associated DNA helicase activity, J. Biol. Chem. 263 (1) (1988) 383–392.
[49] Y. Murakami, J. Hurwitz, Functional interactions between SV40 T antigen and other replication proteins at the replication fork, J. Biol. Chem. 268 (15) (1993) 11008–11017.
[50] R. Vlijm, A. Mashaghi, S. Bernard, M. Modesti, C. Dekker, Experimental phase diagram of negatively supercoiled DNA measured by magnetic tweezers and fluorescence, Nanoscale 7 (7) (2015) 3205–3216.
[51] Jan Lipfert, Xiaomin Hao, Nynke H. Dekker, Quantitative modeling and optimization of magnetic tweezers, Biophys. J. 96 (12) (2009) 5040–5049.